PHYSICS AND CHEMISTRY OF SOLID STATE
V. 27, No.2 (2026) pp. 272-278
Section: Chemistry

DOI: 10.15330/pcss.27.2.272-278

Vasyl Stefanyk Carpathian National University

ФІЗИКА І ХІМІЯ ТВЕРДОГО ТІЛА
Т. 27, № 2 (2026) С. 272-278
Хімічні науки

UDC: 546:548.736.3

ISSN 1729-4428 (Print)
ISSN 2309-8589 (Online)

A. Ivanushko[1], H. Ünsal[2], V. Babizhetskyy[1], O. Zaremba[1], A. Zelinskiy[1], K. Miliyanchuk[1], P. Tatarko[2], R. Gladyshevkii[1]

Enhanced B4C-based materials with TiB_2 additive prepared by spark plasma sintering

[1]*Department of Inorganic Chemistry, Ivan Franko National University of Lviv, Lviv, Ukraine* andriana.ivanushko@lnu.edu.ua
[2]*Institute of Inorganic Chemistry, Slovak Academy of Sciences, Bratislava, Slovak Republic*

B_4C–TiB_2 ceramic materials were prepared by spark plasma sintering of powder mixtures B_4C+TiB_2 (12 wt.%) in an argon atmosphere at 1900°C and a uniaxial pressure of 70 MPa. X-ray powder diffraction was used for the phase analysis and to refine the crystal structures of the individual phases. The influence of homogenization of the initial powders (using ball milling) on the mechanical properties of the ceramics was studied. Vickers hardness values of 38.8 GPa (without ball milling) and 41.1 GPa (ball-milled starting powders) for B_4C–TiB_2 composites were reached and the relative density of the samples exceeded 99 %.

Keywords: Boron carbide, Spark plasma sintering, X-ray powder diffraction, Hardness.

Received 16 November 2025; Accepted 20 April 2026; Published 24 April 2026.

Introduction

Among the priority tasks of modern research is the design of alternative superhard materials with an appropriate set of chemical, mechanical, and thermal properties for application in mechanical engineering, construction, mining, medicine, as well as in the military industry.

Hardness gives ceramics unique ballistic characteristics that provide them with advantages over lighter polymer laminates and cheaper high-hardness steels. Three main classes of ceramics have proven themselves for use in body armor: aluminum oxide (corundum) Al_2O_3, silicon carbide SiC, and boron carbide B_4C. In this sequence, the ballistic qualities become better, but at the same time the price increases. Armor elements made of B_4C-based materials are currently the most effective and reliable ones.

B_4C has high hardness (only slightly inferior to diamond C and boron nitride BN) and low density (~2.52 g/cm^3) [1]. Modern research suggests using additives to increase the relative density, control the grain growth, and improve the mechanical properties of B_4C-based ceramic materials. A literature survey drew our attention to B_4C–TiB_2 ceramic materials as having strong potential. The B_4C–TiB_2 composites were obtained by classical hot pressing [2] or by the modern and faster method of spark plasma sintering (SPS) [3,4].

The aim of this work was to obtain high-quality B_4C-based ceramics with TiB_2 additive (B_4C–TiB_2 composite materials) by the spark plasma sintering method.

I. Starting materials and experimental methods

B_4C-based ceramic materials were prepared starting from high-purity B_4C and TiB_2 powders. The composition of B_4C used here as obtained from an earlier Rietveld refinement was $B_{13.12(2)}C_{1.75(1)}$ [5], *i.e.* close to that of the ordered model $B_{13}C_2$. According to the literature, the homogeneity range of "B_4C" extends from $B_4C_{0.34}$ to $B_4C_{0.96}$, however, for convenience, the phase will here be referred to by its commonly used name B_4C. The amount of TiB_2 added to the B_4C powder was 12 wt.%.

Ceramic composites were prepared from a charge of (a) conventionally mixed powders and (b) powders that had been additionally homogenized in a planetary ball mill (PM100, Retsch) in a WC jar with WC balls (diameter 10 mm) for 20 min at a speed of 250 rpm. Scanning electron microscopy (SEM) images of the starting powders are shown in Fig. 1. The average grain size was 1.20 μm for the initial (not ball-milled) B_4C, 0.84 μm for the initial (not ball-milled) TiB_2 powder, and 1.13 μm and 0.81 μm, respectively, in the ball-milled homogenized mixture B_4C+TiB_2.

The powder mixtures were submitted to spark plasma sintering (SPS). This method uses a pulsed electric current and uniaxial mechanical pressure to densify the sample and allows quick consolidation of ceramics at lower temperatures than what is usual by hot pressing or sintering in a resistance furnace. The SPS method and the equipment used here have been described in details elsewhere, *e.g.* [6]. The SPS was carried out in an argon atmosphere at a maximum temperature of 1900°C and a pressure of 70 MPa. A technological scheme of the synthesis is shown on Fig. 2. The final pellets had a diameter of ~20 mm and were ~5 mm thick.

SEM images were obtained with a Tescan Vega 3 LMU scanning electron microscope (Oxford Instruments AZtecOne System, X-Max^{N}20 detector). Energy-dispersive X-ray (EDX) analysis (qualitative and quantitative element analysis) was also performed. The grain size was evaluated using ImageJ software [7].

X-ray powder diffraction patterns from the surface of the synthesized pellets were collected on a DRON 2.0M powder diffractometer (Fe *K*α-radiation). Structure analyses were performed by Rietveld refinement using the FullProf Suite software [8].

The density of the ceramic material was determined by hydrostatic weighing according to Archimedes' principle using an analytical electronic balance.

Hardness (by Vickers method) was measured with a square-based diamond pyramidal indenter (included angle 136° opposite faces) and a load of 1 kgf (9.807 N) (Novotest TS-MKV1).

II. Results and discussion

The results of the X-ray diffraction of the B_4C-based ceramics with TiB_2 additives (synthesized without and with ball milling of the starting powders) are presented in

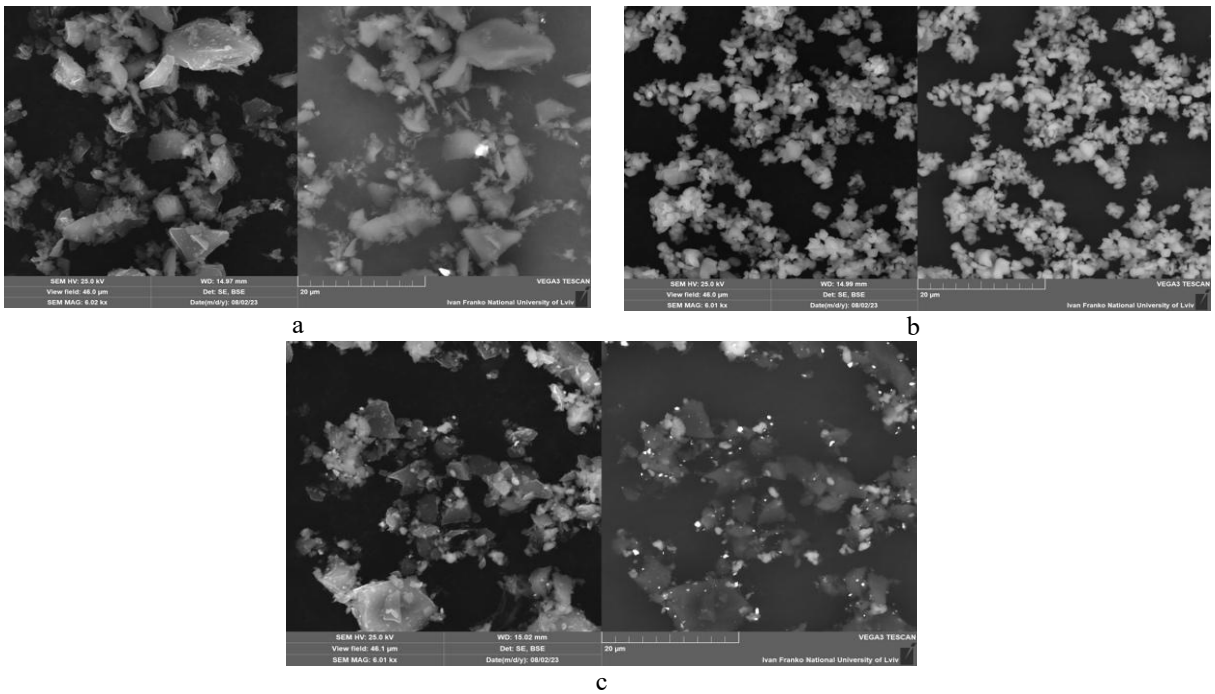

Fig. 1. SEM images of (a) initial B_4C, (b) initial TiB_2, and (c) ball-milled mixture B_4C+TiB_2.

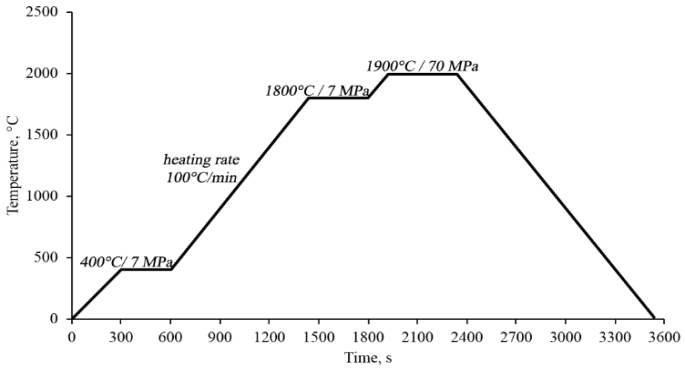

Fig. 2. Technological scheme of the synthesis.

Table 1 and Fig. 3. Both samples contained the two initial phases, B_4C and TiB_2. The relative amounts according to the Rietveld refinement were 96.4(12)/3.6(1) wt.% and 89.1(18)/10.9(2) wt.% for the materials B_4C–TiB_2 without and with ball milling of the starting powders, respectively. A comparison with the initially added amount of 12 wt.% TiB_2, showed a less homogenous distribution of the phases in the sample that had not been submitted to ball milling. In both cases the refined cell parameters are close to those of the starting materials and to the values reported in the literature. Complete refinements were carried out using 41 reflections for the B_4C phase and 9 reflections for TiB_2.

Several models have been proposed in the literature to describe the disorder occurring in the crystal structure of B_4C [9]. The model selected here was used for an earlier refinement of pure B_4C [5] and allows a slight deviation towards the B-rich side compared to the stoichiometric composition $B_{13}C_2$. The crystal structure of $B_{13}C_2$ contains four crystallographically independent atomic positions in space group *R*-3*m*. The basic units of the structure are empty icosahedra formed by boron atoms, B_{12} (sites B1 and B2), interconnected *via* external B-B bonds and three-atom linear units C-B-C (sites C and B4), oriented along [001]. The C atoms center B_4 tetrahedra formed by the B atom at 0 0 0 (site B4) and three B atoms from three different icosahedra. Deviations from the ideal

Table 1.

Results of the Rietveld refinements of the ceramic materials B_4C–TiB_2, compared with pure B_4C submitted to a similar treatment [5]

Refined composition, space group, cell parameters, R_B	Site	Wyckoff position	*x*	*y*	*z*	B_{iso}, Å^2	Occ.
B_4C ceramic material (without ball milling) (R_p = 6.10 %, R_{wp} = 8.04 %) [5]							
$B_{13.12(2)}C_{1.75(1)}$ *R*-3*m* *a* = 5.60333(15) Å, *c* = 12.0926(5) Å, *V* = 328.809(18) Å^3 R_B = 6.95 %	B1	18*h*	0.44196(16)	0.55804(16)	0.04756(17)	1.38(5)	1
	B2	18*h*	0.50683(17)	0.49317(17)	0.1926(2)	1.58(4)	1
	C	6*c*	0	0	0.1209(7)	1.38(12)	0.877(5)
	B3	6*c*	0	0	0.102(7)	1.38(12)	0.123(5)
	B4	3*a*	0	0	0	1.38(12)	0.877(5)
B_4C–TiB_2 ceramic material (without ball milling) (R_p = 4.33 %, R_{wp} = 5.73 %)							
$B_{13.156(14)}C_{1.688(10)}$ *R*-3*m* *a* = 5.6111(2) Å, *c* = 12.1064(6) Å, *V* = 330.10(3) Å^3 R_B = 6.97 %	B1	18*h*	0.4415(2)	0.5585(2)	0.0495(2)	1.66(6)	1
	B2	18*h*	0.5064(2)	0.4936(2)	0.1934(3)		1
	C	6*c*	0	0	0.1214(4)		0.844(5)
	B3	6*c*	0	0	0.097(19)		0.156(5)
	B4	3*a*	0	0	0		0.844(4)
TiB_2: *P*6/*mmm*, *a* = 3.03721(16) Å, *c* = 3.2410(2) Å, *V* = 25.891(3) Å^3, R_B = 7.16%							
B_4C–TiB_2 ceramic material (ball-milled starting powders) (R_p = 3.99 %, R_{wp} = 5.36 %)							
$B_{13.07(2)}C_{1.870(16)}$ *R*-3*m* *a* = 5.6105(3) Å, *c* = 12.1047(8) Å, *V* = 329.98(4) Å^3 R_B = 10.1 %	B1	18*h*	0.4412(3)	0.5588(3)	0.0504(4)	1.69(10)	1
	B2	18*h*	0.5044(4)	0.4956(4)	0.1921(6)		1
	C	6*c*	0	0	0.1219(7)		0.935(8)
	B3	6*c*	0	0	0.101(7)		0.065(8)
	B4	3*a*	0	0	0		0.935(8)
TiB_2: *P*6/*mmm*, *a* = 3.0415(2) Å, *c* = 3.2328(2) Å, *V* = 25.899(3) Å^3, R_B = 5.95%							

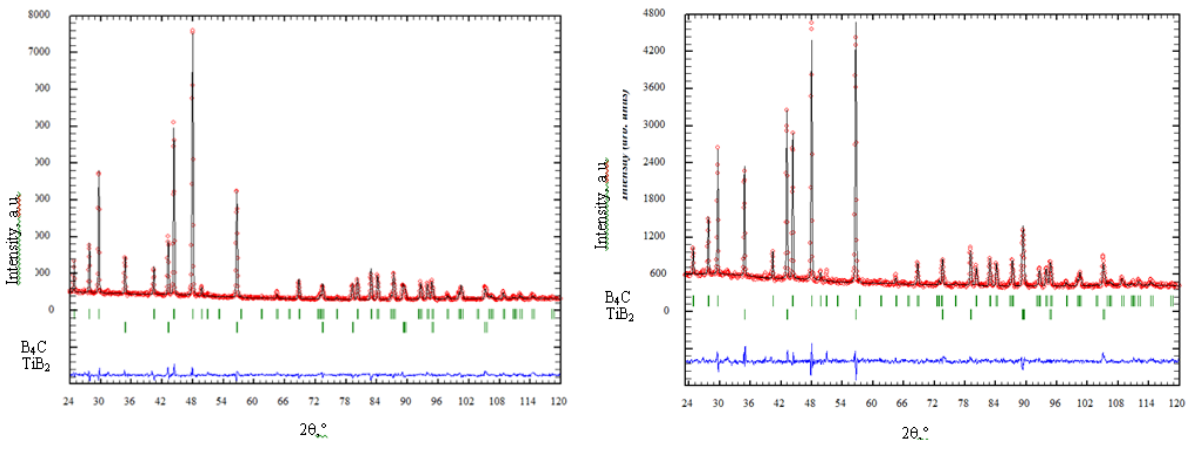

a b

Fig. 3. Observed, calculated, and difference XRD patterns (Fe *K*α-radiation of the (a) B_4C–TiB_2 (without ball milling) and (b) B_4C–TiB_2 (ball-milled starting powders) ceramic materials. The positions of the reflections from B_4C and TiB_2 are indicated by bars.

composition are achieved by partial replacement of C-B-C units by B-B pairs (site B3). Fig. 4 shows a perspective view of the structure, ignoring site B3. The occupancies of the partly occupied sites were restrained as follows: occ(B4) = occ(C) = 1 – occ(B3). Interatomic distances in the crystal structure of B_4C [5] are listed in Table 2. The distance B3-B3 is relatively long. An additional boron site in Wyckoff position 36*i* is sometimes proposed to occupy the space around 0 0 0 when B4 is absent [9], however, the very low occupancy factor does not allow it to be considered here.

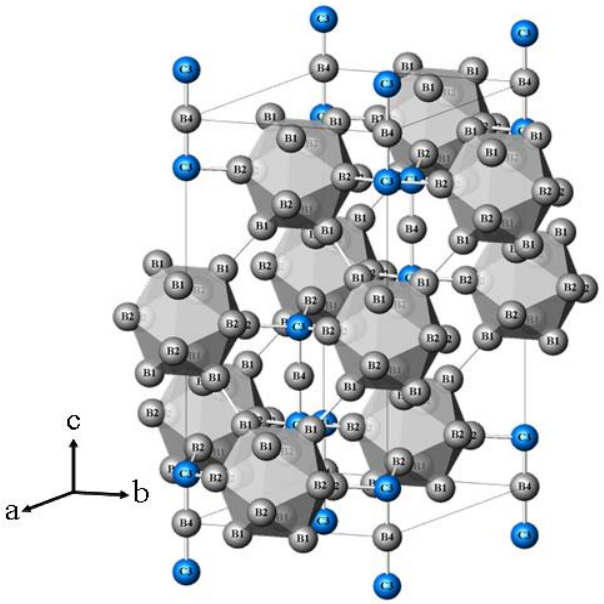

Fig. 4. Arrangement of boron icosahedra and C-B-C units in the crystal structure of ordered $B_{13}C_2$ (B_4C) (B atoms – grey, C atoms – blue).

Table 2.

Interatomic distances in the crystal structure of $B_{13.12(2)}C_{1.75(1)}$ [5]. Impossibly short distances involving the partly occupied sites C, B3, and B4 are omitted.

Site		Distance δ, Å
B1	1 B1	1.610(2)
	2 B1	1.8260(14)
	2 B2	1.855(2)
	1 B2	1.863(3)
B2	1 C [a]	1.5697(17)
	1 B3 [a]	1.62(2)
	2 B2	1.7968(16)
	2 B1	1.855(2)
	1 B1	1.863(3)
C	1 B4	1.462(8)
	3 B2	1.5697(17)
B3	3 B2	1.62(2)
	1 B3	2.47(12)
B4	2 C	1.462(8)

[a] either 1 C or 1 B3

The model for the refinement of TiB_2 was taken from Pearson's Crystal Data [9]. The crystal structure belongs to the structure type AlB_2 (space group *P6/mmm*, atomic coordinates Ti 1*a* (0 0 0), B 2*d* (⅓ ⅔ ½)).

The B_4C–TiB_2 materials were investigated by energy-dispersive X-ray spectroscopy and scanning electron microscopy. SEM images and elemental mapping of the samples are shown in Fig. 5. The results confirm the homogeneity of the materials. For both materials the grain size of the minority phase TiB_2 was evaluated, taking into consideration more than 92 % of the total number of particles. The graphs in Fig. 5 show smaller grains (peak at 0.5-1.0 μm) and then a more homogeneous distribution of grains of different sizes for the material prepared from

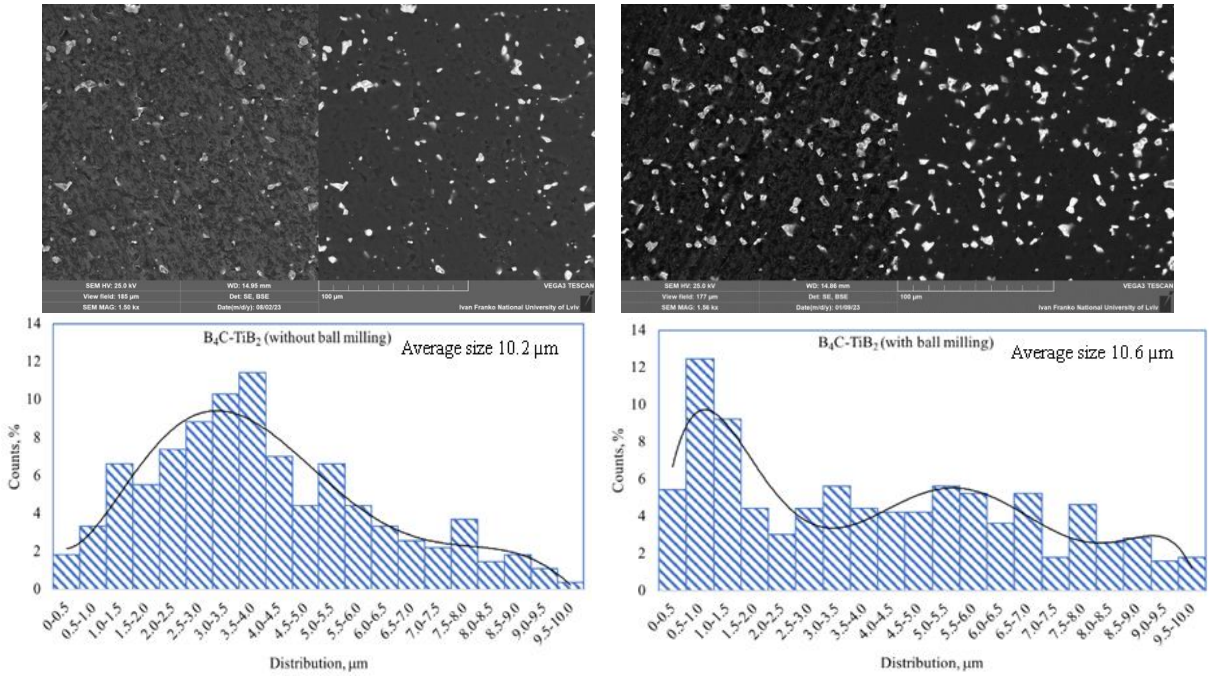

a b

Fig. 5. SEM images and grain-size distributions of the TiB_2 phase for (a) B_4C–TiB_2 (without ball milling) and (b) B_4C–TiB_2 (ball-milled starting powders) ceramic materials.

ball-milled powder. The size distribution for the sample prepared without ball-milling exhibits a closer to gaussian shape with the maximum at 3.0 µm. Elemental mapping for the B_4C–TiB_2 ceramic materials is shown in Fig. 6.

Vickers hardness was measured to see the effect of the addition of TiB_2 and ball milling. A comparison of literature data indicates that the introduction of TiB_2 into the B_4C matrix contributes to an increase in the hardness; however, this effect depends on the amount of additive and the sintering conditions. For B_4C ceramics prepared by spark plasma sintering at 2000°C and a pressure of 70 MPa, the hardness reached 32.6 GPa for a relative density of 99.5 % [5]. According to Rubink *et al.* [3], a B_4C – 13 vol.% (~17.5 mol.%) TiB_2 composite obtained at 1900°C and 50 MPa exhibited a hardness of about 35 GPa for a relative density of 99.4 %, whereas on increasing the TiB_2 content to 23 vol.% (~30 mol.%) the hardness decreased to 33 GPa (density 99.5 %). The B_4C – 5 vol.% (~7 mol.%) TiB_2 composite synthesized by Uygun *et al.* [4] at a lower temperature, 1760°C, and a pressure of 40 MPa showed a hardness of 34.5 GPa and a relative density of 98.1 %. The materials investigated in this work, namely a B_4C – 12 wt.% (~10 mol.%) TiB_2 composite synthesized at 1900°C and 70 MPa, exhibited a hardness of 38.8 GPa and a relative density of 99.0 %. The use of ball milling for mixing the initial powder further increased the hardness to 41.1 GPa for a density of 99.5 %. Thus, the composites obtained here exhibit higher hardness than pure B_4C and most B_4C–TiB_2 materials reported in the literature, which may be attributed to the optimal TiB_2 content, the higher pressure applied during SPS, and a more homogeneous distribution of the additive. The synthesis temperature, relative density and hardness of the synthesized ceramic composites are summarized in Table 3.

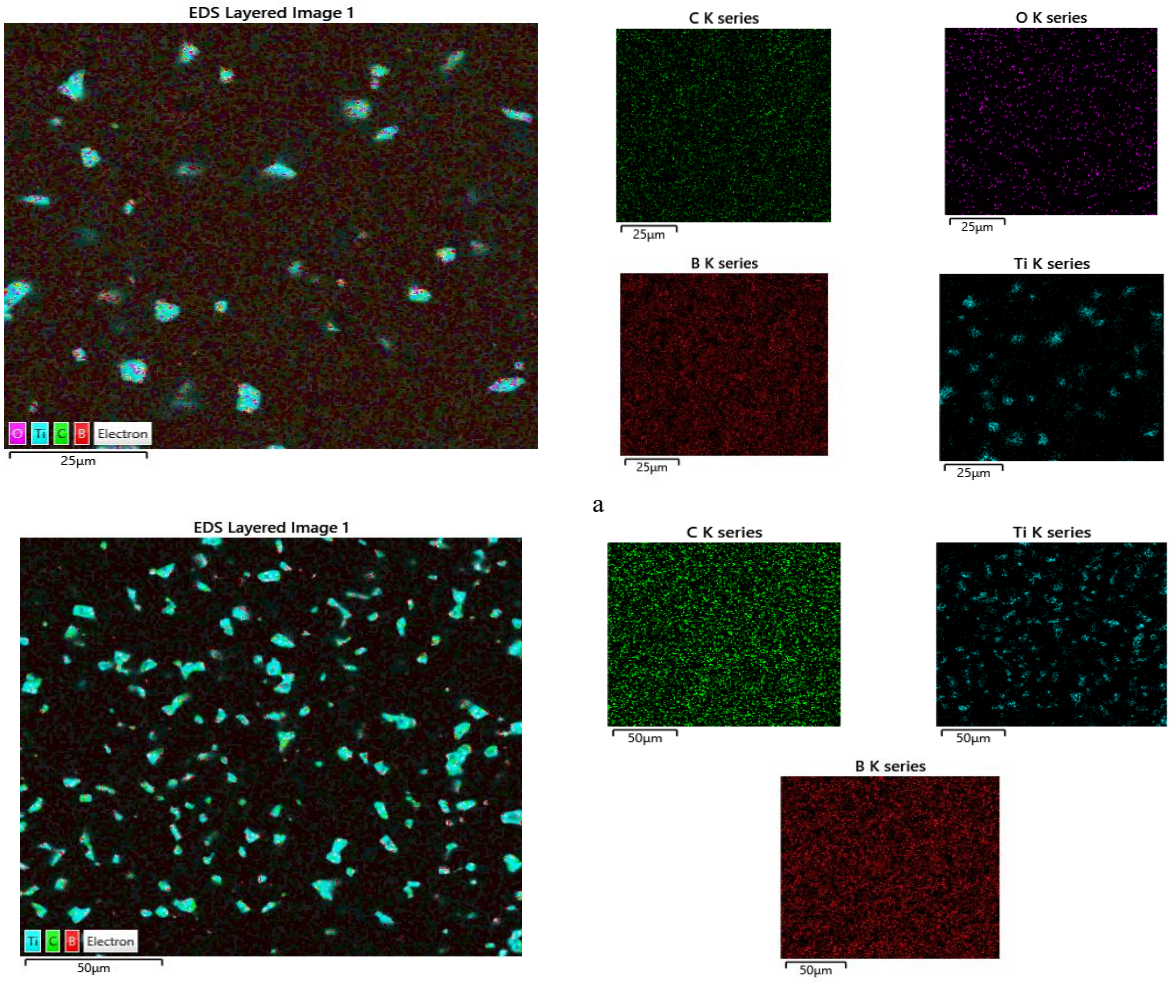

Fig. 6. Elemental mapping for the B_4C–TiB_2 ceramic materials obtained without (a) and with (b) ball milling of the starting powders.

Table 3.

Initial composition, synthesis conditions, relative density, and hardness of the ceramic composites

Composite	TiB_2 content, wt.%	SPS temperature, °C	Ball milling	Relative density, %	Hardness, HV1	Hardness, GPa
B_4C [5]	–	2000	no	99.5	3320	32.6
B_4C–TiB_2	12	1900	no	99.0	3954	38.8
B_4C–TiB_2	12	1900	yes	99.5	4188	41.1

Conclusions

Two B_4C–TiB_2 ceramic materials were prepared by SPS, one from conventionally mixed powders, the other one from ball-milled powders. X-ray powder diffraction (Rietveld refinement) confirmed the presence of the phases B_4C and TiB_2 in both materials, however, with a phase ratio close to the nominal composition (12 wt.%) only in the case of the ceramic material prepared from ball-milled powders. Microstructure investigations showed that preliminary ball milling of the powder mixture had led to a more homogeneous distribution of the additive.

It was shown that the addition of TiB_2 increases the hardness of the composites in comparison with pure B_4C. The B_4C–12 wt.% TiB_2 material obtained without ball-milling the starting powders exhibited a hardness of 38.8 GPa for a relative density of 99.0 %, and by using ball milling the hardness could be increased to 41.1 GPa for a relative density of 99.5 %. The enhancements may be attributed to an optimized TiB_2 content, a higher pressure (70 MPa) applied during the sintering, and improved homogeneity of the material.

A.I. greatly acknowledge the support by the Ministry of Science and Education of Ukraine (grant No. 0125U000767).

H.U. and P.T. greatly acknowledge the support of the VEGA project No. 2/0133/26 and SAS-TUBITAK/JRP/2023/807/HiTemCom (No. 720464).

Andriana Ivanushko – Ph.D. student at the Department of Inorganic Chemistry;
Hakan Ünsal – Ph.D., Researcher at the Ceramic Department;
Volodymyr Babizhetskyy – Dr.Sc., Leading Researcher at the Department of Inorganic Chemistry;
Oksana Zaremba – Ph.D., Associate Professor at the Department of Inorganic Chemistry;
Anatoliy Zelinskiy – Ph.D., Senior Researcher at the Department of Inorganic Chemistry;
Khrystyna Miliyanchuk – Ph.D., Associate Professor at the Department of Inorganic Chemistry;
Peter Tatarko – Ph.D., Senior Researcher at the Ceramic Department;
Roman Gladyshevkii – Academician of the NAS of Ukraine, Dr.Sc., Professor at the Department of Inorganic Chemistry.

[1] I.G. Crouch, *Body armour – new materials, new systems*, Def. Technol., 15, 241 (2019); https://doi.org/10.1016/j.dt.2019.02.002.
[2] A. K. Suri, C. Subramanian, J. K. Sonber, T. S. R. Ch. Murthy, *Synthesis and consolidation of boron carbide: a review*, Int. Mater. Rev., 55(1) 4 (2010); https://doi.org/10.1179/095066009X12506721665211
[3] W. S. Rubink, V. Ageh, H. Lide, N. A. Ley, M. L. Young, D. T. Casem, E. J. Faierson, T. W. Scharf, *Spark plasma sintering of B_4C and B_4C–TiB_2 composites: deformation and failure mechanisms under quasistatic and dynamic loading*, J. Eur. Ceram., Soc. 41(6) 3321 (2021); https://doi.org/10.1016/j.jeurceramsoc.2021.01.044.
[4] B. Uygun, G. Göller, O. Yücel, F. Çinar Şahin, *Production and characterization of boron carbide – titanium diboride ceramics by spark plasma sintering method,* Adv. Sci. Technol., 63, 68 (2010); https://doi.org/10.4028/www.scientific.net/AST.63.68.
[5] A. Ivanushko, R. Gladyshevskii, *B_4C ceramic prepared by spark plasma sintering*, Visn. Lviv. Univ. Ser. Khim., 65, 102 (2024); http://dx.doi.org/10.30970/vch.6501.102.
[6] H. Ünsal, S. Grasso, A. Kovalčíková, O. Hanzel, M. Tatarková, I. Dlouhý, P. Tatarko, *In-situ graphene platelets formation and its suppression during reactive spark plasma sintering of boron carbide/titanium diboride composites*, J. Eur. Ceram. Soc., 41 6281 (2021); https://doi.org/10.1016/j.jeurceramsoc.2021.06.053.
[7] W. Rasband, ImageJ (Version 1.51), National Institute of Mental Health, Bethesda, Maryland, USA. https://imagej.nih.gov/ij/index.html.
[8] J. Rodriguez Carvajal, *Recent Developments of the Program FULLPROF, in Commission on Powder Diffraction (IUCr)*, Newsletter, 26, 12 (2001); http://journals.iucr.org/iucr-top/comm/cpd/Newsletters/.
[9] P. Villars, K. Cenzual (Eds.), *Pearson's Crystal Data – Crystal Structure Database for Inorganic Compounds*, ASM International, Materials Park (OH), (2024/2025); https://www.crystalimpact.com/pcd/.

А. Іванушко[1], Х. Унсал[2], В. Бабіжецький[1], О. Заремба[1], А. Зелінський[1],
Х. Міліянчук[1], П. Татарко[2], Р. Гладишевський[1]

Синтез методом іскроплазмового спікання матеріалів на основі B_4C, покращених додаванням TiB_2

[1]*Кафедра неорганічної хімії, Львівський національний університет імені Івана Франка, Львів, Україна,* andriana.ivanushko@lnu.edu.ua
[2]*Інститут неорганічної хімії, Словацька академія наук, Братислава, Словацька Республіка*

Методом іскроплазмового спікання за максимальної температури 1900°C та тиску 70 МПа синтезовано композитні матеріали B_4C–TiB_2 із суміші вихідних порошків B_4C і TiB_2 (12 мас.%) без та з додатковою обробкою у планетарному кульовому млині. Після синтезу обидна зразки містили фази B_4C і TiB_2, що підтверджено рентгенівською дифракцією та енергодисперсійною рентгенівською спектроскопією. За результатами рентгенівської порошкової дифракції уточнено кристалічну структуру індивідуальних фаз у синтезованих керамічних матеріалах. Методом скануючої електронної мікроскопії досліджено отримані керамічні матеріали і вихідні порошки. Встановлено середній розмір зерен фази TiB_2 в композитному матеріалі та середні розміри частинок вихідних порошків. Методом Віккерса визначено твердість композитних матеріалів B_4C–TiB_2 без та з додатковою обробкою суміші вихідних порошків у планетарному кульовому млині, що становить 38,8 та 41,1 ГПа, відповідно, при відносній густині 99,0 та 99,5 %.

Ключові слова: Борокарбід, Іскроплазмове спікання, Рентгенівська порошкова дифракція, Твердість.